Journal of Materials Chemistry B

PAPER

View Article Online
View Journal | View Issue

Cite this: J. Mater. Chem. B, 2015, 3, 1335

Porphyrin functionalized porous carbon derived from metal–organic framework as a biomimetic catalyst for electrochemical biosensing

Pinghua Ling, Qing Hao, Jianping Lei* and Huangxian Ju

Received 29th September 2014
Accepted 18th December 2014

DOI: 10.1039/c4tb01620c

www.rsc.org/MaterialsB

In this work, a kind of biomimetic catalyst was designed as a signal probe by the assembly of porphyrin on porous carbon (PC) derived from metal–organic frameworks for electrochemical biosensing. First, PC was prepared by direct carbonization of a zeolite-type metal–organic framework as both a precursor and a template, and characterized by transmission electron microscopy, nitrogen sorption isotherm, X-ray photoelectron spectroscopy and X-ray diffraction. Then the PC was non-covalently functionalized with iron(III) meso-5,10,15,20-tetrakis(4-carboxyphenyl) porphyrin chloride (FeTCPP) *via* non-covalent interactions. The resulting nanocomposite of PC/FeTCPP possesses an excellent electrocatalytic activity toward oxygen reduction. Coupling with the enzymatic catalysis of glucose oxidase, a glucose biosensor was constructed on the basis of O_2 consumption. The biomimetic sensor enables a reliable and sensitive determination of glucose with a linear range of 0.5 to 18 mM and a detection limit of 0.08 mM at a signal-to-noise ratio of 3. Moreover, the biosensor exhibits the analytical reproducibility and stability with a lower relative standard deviation of 4.2%. In an application to detect glucose in human serum samples, this glucose biosensor had good detection accuracy with analytical recoveries from 97.3% to 107.7%. Therefore, the porphyrin functionalized PC provides a promising biomimetic platform for constructing the biosensors, and has potential application in bioanalysis and clinical diagnosis.

Introduction

Artificial mimetic catalysts have been extensively investigated as low-cost alternatives to natural enzymes in the last decade. Compared with natural enzymes, artificial mimetic catalysts are more conveniently synthesized and more easily modified.[1,2] More significantly, artificial mimetic catalysts can sustain their stability and catalytic activity even over a wide range of temperatures (4–90 °C) and pH (0–12).[3] The conventional artificial mimetic materials such as cyclodextrins, metal complexes, polymers and fullerene derivatives have been successfully applied to mimic the structures and functions of natural enzymes.[4–8] A variety of nanomaterials including gold nanoparticles, rare earth nanoparticles and ferromagnetic nanoparticles have also been found to exhibit unexpected enzyme-like activity owing to their unique chemical and physical characteristics.[9–17]

Recently, porphyrins, as the analogues of the active site of enzymes, are considered to be the efficient mimics of many important enzymes.[18–22] In particular, iron porphyrin is the mimic of cytochrome c oxidase, which shows good electrocatalysis towards biologically important molecules.[23,24] However, there is limited use of porphyrins in electrochemical biosensing owing to their poor conductivity.[25] The immobilization of porphyrins on nanomaterials such as graphene,[26] carbon nanotubes[27] and carbon nanohorns[19] provides a promising approach to enhance the electrochemical catalysis due to their good conductivity.[28,29] For example, the ordered ultrathin films based on layered double hydroxide nanoplatelets and manganese porphyrin have been utilized as an electrochemical sensor for glucose.[30] Mulchandani *et al.*[31] have fabricated a single-walled carbon nanotube-porphyrin hybrid for monitoring volatile organic compounds in air. In this work, a novel biomimetic catalyst was designed by the assembly of porphyrin on porous carbon derived from metal–organic frameworks (MOFs) for electrochemical biosensing.

Porous carbon materials have been used in many research fields due to their unique properties such as high surface area, large pore volume and good electrochemistry.[32–40] They are often synthesised using electrical arc,[41] laser ablation,[42] chemical vapor decomposition[43] as well as chemical or physical activation methods.[44] However, these methods usually involve rigorous reaction conditions, and thus are difficult to control the sizes of the pore. Alternatively, nanoporous carbon materials could be synthesized by direct carbonization of MOFs to yield crystalline molecular materials with an unprecedentedly large and permanent inner porosity.[45–47] The pore sizes of MOF structures are easily controlled through the design of specific ligands and

State Key Laboratory of Analytical Chemistry for Life Science, School of Chemistry and Chemical Engineering, Nanjing University, Nanjing 210093, P.R. China. E-mail: jpl@nju.edu.cn; Fax: +86 25 83593593; Tel: +86 25 83593593

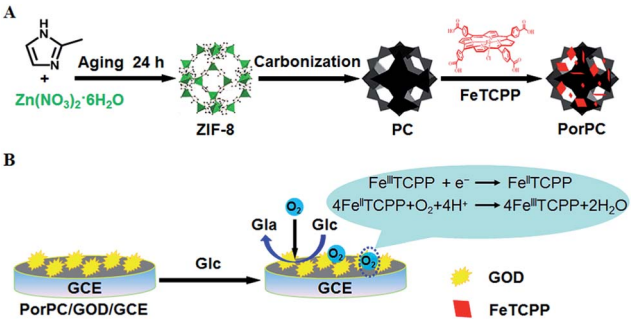

Scheme 1 Schematic representation of (A) preparation of PorPC and (B) sensing mechanism for electrochemical detection of glucose.

doping metal ions in the frame, which should constitute an important advantage over other conventional chemo-sensory materials.[48] For example, Yaghi *et al.*[49] designed an oligo-ethylene glycol-functionalized MOF-74 structure, which is large enough for natural proteins to enter the pores. Thus MOFs can be employed as the templates and carbon precursors during the synthesis of porous carbon.[50,51] Moreover, the incorporation of heteroatoms such as nitrogen into the carbon nanomatrix can enhance the thermal/chemical stability and hydrophilic properties.[52–55] The unique electronic interactions between the lone-pair electrons of nitrogen and the π system of graphitic carbon in these N-decorated porous carbons result in good electrocatalytic activity towards oxygen reduction.[56,57] Thus it is desired to use porous carbon derived from MOFs as a supporter and electron accelerator for electrochemical biosensing.

Here, we have used an N-rich MOF with a zeolite-type framework (ZIF-8),[58,59] as both a template and a precursor to synthesis N-decorated porous carbon. Porphyrin was conjugated to porous carbon (PC) through π–π noncovalent interactions to form the porphyrin-porous carbon nanocomposite (PorPC) (Scheme 1A). As shown in Scheme 1B, a systematic study was carried out to evaluate the electrocatalytic activity of the nanohybrid toward oxygen reduction. Using glucose oxidase as a model, a glucose (Glc) biosensor on the basis of O_2 consumption was constructed with good sensing performance. The present work provides a novel example of the assembly of porphyrin into porous carbon in the field of biosensing.

Experimental

Reagents and materials

All commercial reagents were acquired in high purity and used without further purification: Zinc nitrate ($Zn(NO_3)_2 \cdot 6H_2O$), 2-methylimidazole, methanol, and glucose oxidase (GOD, EC 1.1.3.4, type X-S, lyophilized powder, 100–250 units mg^{-1}, from *Aspergillus niger*) were purchased from Sigma-Aldrich. Iron(III) meso-5,10,15,20-tetrakis(4-carboxyphenyl)porphyrin chloride (FeTCPP) was obtained from J&K Scientific Ltd. (China). Ascorbic acid (AA), uric acid (UA), and D-(+)-glucose were bought from Sinopharm Chemical Reagent Co. Ltd. (China). Nafion (product no. 274704) was purchased from Aldrich. In our work, 0.1 M phosphate buffer salines (PBS) at various pH values were prepared by mixing stock standard solutions of Na_2HPO_4 and KH_2PO_4, and then adjusted to the required pH value with 0.1 M HCl or NaOH. Ultrapure water obtained from a Millipore water purification system (Milli-Q, ≥18.2 MΩ) was used throughout the experiments. The glucose stock solution was allowed for mutarotation by overnight storage at room temperature prior to use. The GOD solution (2 mg mL^{-1}) was prepared in 0.1 M PBS of pH 7.0 and stored at 4 °C. Human blood serum samples were generously provided by Jiangsu province tumor hospital.

Characterization

X-ray diffraction (XRD) was equipped with a Cu sealed tube (λ = 1.54178 Å) at 40 kV and 40 mA. Scanning electron micrographs (SEMs) were recorded on a Hitachi S-4800 scanning electron microscope (Hitachi, Japan) and transmission electron micrographs (TEMs) were acquired using a JEOL JEM-2010 transmission electron microscope operating at an accelerating voltage of 200 kV. X-ray photoelectron spectroscopy (XPS) was carried out using an ESCALAB 250 spectrometer (Thermo-VG Scientific Co., U.S.A.) with ultra-high vacuum generators. The nitrogen sorption isotherms of porous carbon were obtained through Brunauer–Emmett–Teller on a Micromeritics ASAP2020. Cyclic voltammetric (CV) experiments were conducted on a CHI 660D electrochemical workstation (Shanghai CH Instruments, China) with a three-electrode system consisting of a glassy carbon electrode (GCE) as a working electrode, a saturated calomel electrode (SCE) as a reference electrode (Caution: calomel is toxic) and a platinum wire as a counter electrode.

Synthesis of ZIF-8 based porous carbon

According to a reported procedure with some modification,[54,60] the hierarchically porous carbon was prepared from the ZIF-8 material. Typically, 1.29 g of $Zn(NO_3)_2 \cdot 6H_2O$ was dissolved in 100 mL methanol under stirring to prepare a solution and 1.32 g of 2-methylimidazole was dissolved in 100 mL methanol to prepare another solution. Then, the latter solution was added to the former solution and stirred for 5 min, the resulting mixture was allowed to age overnight at room temperature. After that, the white precipitate was filtered and washed with methanol several times to remove any externally adsorbed 2-methylimidazole and dried under vacuum before further use. The prepared ZIF-8 powder was transferred into a quartz boat, placed in a furnace under a N_2 flow, and heated at 800 °C for 5 h with a heating rate of 5 °C min^{-1}. Next, the sample was vigorously washed with HCl solution (2 M) and also several times with distilled water, and dried under vacuum at 120 °C for 24 h.

Preparation of PorPC and biosensors

In our procedure, 6 mg of porous carbon was dispersed in 5 mL of ultrapure water. Then the suspension was successively added to a FeTCPP dimethylformamide-water mixture (1 mL, 2 mM), before being ultrasonically dispersed for 1 h, and centrifuged at 10 000 rpm for 20 min to remove free FeTCPP with ultrapure water 5 times. The resulting sample was dried under vacuum at 70 °C for 12 h to obtain the PorPC nanocomposite. The prepared

composite (1 mg) was ultrasonically redispersed in ultrapure water (1 mL) for further experiments.

Before use, the GCEs were polished with a slurry of alumina oxide powder (1.0 and 0.05 μm) on chamois leather, respectively, washed ultrasonically and dried at room temperature. Next, 5 μL of PorPC water suspension (1 mg mL^{-1}) was applied to the pretreated GCE surface and this was allowed to dry at room temperature Then the PorPC modified GCE was immersed in 0.1 M PBS containing 2 mg mL^{-1} GOD for 20 h at 4 °C. The PorPC/GOD modified GCE was thoroughly rinsed with ultrapure water to remove the loosely adsorbed enzyme molecules. In order to avoid leakage of PorPC from the surface of the GCE, a drop of 4 μL of 1% Nafion solution was applied on the electrode before electrochemical measurements. All modified electrodes were stored in 0.1 M PBS of pH 7.0 at 4 °C in a refrigerator before use.

Results and discussion

TEM of ZIF-8 crystals reveals that the as-synthesized nanoparticles exhibit the well-known hexagonal ZIF-8 crystal structure of ~100 nm diameter (Fig. 1A), indicating the successful synthesis of ZIF-8 crystals.[47] The prepared ZIF-8 powder was then carbonized at 800 °C for 5 h. Fig. 1B shows the SEM of the carbon material obtained. Here, an intersecting three-dimensional structural feature was observed, which could provide a substantial effective electrode surface area for the loading of biomolecules. The SEM of PorPC in Fig. 1C shows that its morphology was similar to that of porous carbon, indicating that the porous carbon retained the pristine structure after assembly of FeTCPP, which could lead to a highly efficient catalytic activity to oxygen reduction. When GOD was immobilized on the PorPC nanocomposite, the GOD adsorbed on the surface of PorPC and tended to aggregate into island-like structures (Fig. 1D). The open structure of the GOD/PorPC film facilitated the substrate to be accessible to GOD, resulting in a good electrochemical response to glucose.

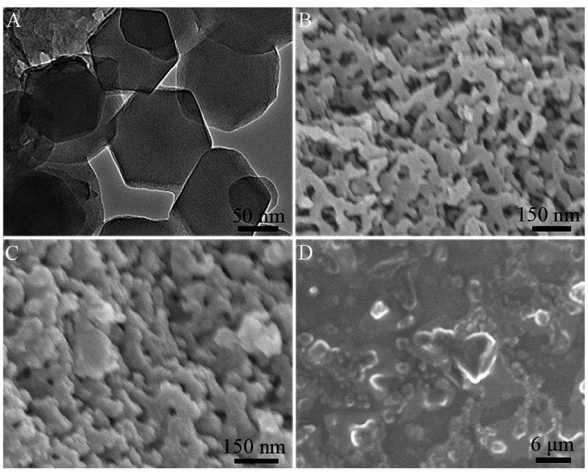

Fig. 1 TEM image of ZIF-8 crystals (A) and SEM images of (B) porous carbon, (C) PorPC, and (D) GOD/PorPC.

A wide-angle XRD pattern of the synthesized porous carbon is shown in Fig. 2. The XRD pattern displays only two broad peaks located at around $2\theta = 25°$ and 44°, that were matched with the carbon (002) and (101) diffractions, respectively,[37] revealing the high purity of the resulting porous carbon. In addition, the weak (002) peak intensity demonstrates a low degree of graphitization, which means a low concentration of parallel single layers in the obtained porous carbon.[61]

XPS was used to investigate the surface composition of porous carbon. As shown in Fig. 3A, the XPS survey spectrum shows intense signals of C1s at 285 eV, N1s at 399 eV and O1s at 531 eV. Based on the XPS results, the nitrogen atomic concentration was estimated to be 4.21% in the porous nanomaterial. Furthermore, the fitted N1s spectrum is divided into three peaks attributed to the different chemical states of N (Fig. 3B): quaternary N (400.8 eV), pyrrolic N (399.4 eV) and pyridinic N (398.2 eV). Therefore, such high contents of N may improve the electrocatalytic activity of porous carbon.[62,63]

Nitrogen sorption experiments were performed to examine the surface areas of the porous carbon and the results obtained are shown in Fig. 4. Both nitrogen adsorption–desorption curves show a typical I-type isotherm, which sharply increases at low relative pressure, suggesting that the micropores are dominant. Meanwhile, the adsorption capacity continually increased at medium relative pressure (Fig. 4A), and the desorption hysteresis denotes the existence of developed mesoporosity. The final almost vertical tail at the relative pressure implies the presence of relatively large cavities.[46,50,60]

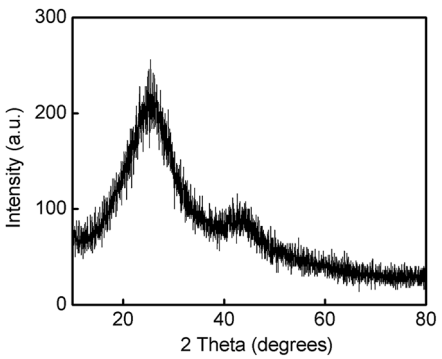

Fig. 2 Wide-angle XRD pattern of the synthesized porous carbon.

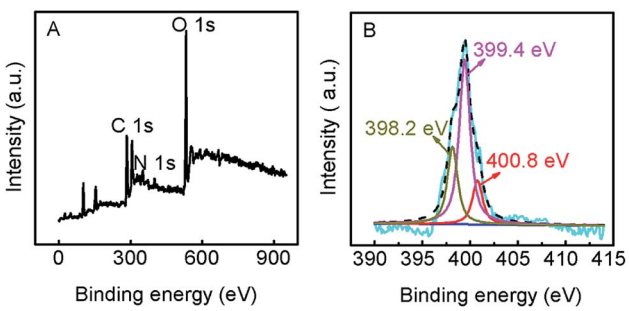

Fig. 3 (A) XPS survey spectrum and (B) N 1s XPS spectrum of porous carbon.

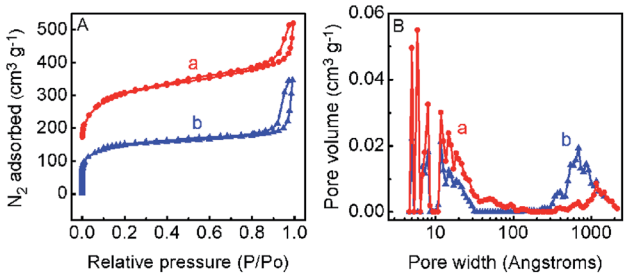

Fig. 4 (A) N_2 adsorption–desorption isotherms and (B) corresponding DFT pore size distribution of (a) PC and (b) PorPC at 77 K.

The porous carbon has a high Brunauer–Emmett–Teller surface area of 1067 m^2 g^{-1} and a pore volume of 0.66 cm^3 g^{-1}, respectively. After being functionalized with FeTCPP, the porous material possesses a surface area of 521 m^2 g^{-1} and a pore volume of 0.34 cm^3 g^{-1}. The decrease in surface area and pore volume was likely to be caused by the loading of FeTCPP in the porous carbon. On the other hand, the corresponding pore size distribution curves of porous carbon and PorPC are shown in Fig. 4B. According to the original density functional theory (DFT), both pore size distributions were mainly centered at 0.5–3 nm, which is suitable for ion diffusion in the aqueous electrolyte.[64]

Fig. 5 shows CVs obtained at different modification stages of electrodes in 0.1 M air-saturated PBS of pH 7.0 at 50 mV s^{-1}. Both the bare GCE (Fig. 5A, curve a) and PC/GCE (Fig. 5A, curve b) showed reduction peaks of O_2 at around −0.6 V.[23] At the PorPC/GCE, a 152% increase in the reduction peak current, compared to PC/GCE, was observed while the reduction potential shifted from −0.6 V to −0.25 V (Fig. 5A, curve c). At the FeTCPP/GCE (Fig. 5A, curve d), there was a 55% decrease in the peak current compared to that at the PorPC/GCE, indicating that the PC can efficiently enhance the catalysis of FeTCPP. Since the catalytic current appeared along with the reduction of FeTCPP, this is a typical electrochemical process followed by a chemical (EC) catalytic process,[65] in which FeTCPP was first reduced to iron(II) species and then back to the initial state by means of a chemical reaction with O_2 (Scheme 1B). These improvements in catalytic activities of PorPC can be explained by the synergistic effects between the efficient electron transfer of porous carbon and the good catalytical active center of iron-porphyrin.

After GOD was immobilized on the PorPC/GCE, the O_2 reduction current peak at the PorPC/GOD/GCE (Fig. 5A, curve e) was 8% smaller than that at the PorPC/GCE. When adding glucose in air-saturated PBS, the O_2 reduction peak current of PorPC/GOD has decreased by 39% (Fig. 5A, curve f), which was attributed to the O_2 consumption *via* the enzyme-catalyzed reaction in the following equation:

$$\text{glucose} + O_2 \xrightarrow{\text{GOD}} \text{gluconolactone} + H_2O_2$$

As a result of O_2 consumption by the GOD catalyzed reaction of glucose, less O_2 was available for reduction at the PorPC/GOD/GCE.

In a separate set of experiments, cyclic voltammetry of nitrogen-saturated buffer was carried out at electrodes (Fig. 5B). At the PorPC/GOD/GCE, the large O_2 reduction peak previously observed has now disappeared, as indicated in curve a, further indicating the reduction current at −0.25 V corresponding to the electrocatalytic reduction of O_2. In order to investigate the effect of H_2O_2, 2.0 mM H_2O_2 was added to nitrogen-saturated PBS, the CV of the PorPC/GCE was a similarly featureless voltammogram in the potential range from −1.0 V to +0.2 V (Fig. 5B, curve b), but a small current difference (~25%) was observed at a more negative potential (<−0.6 V) in response to glucose in air-saturated 0.1 M PBS of pH 7.0 (Fig. 5B, curves c and d), indicating no interference by GOD in the detection of glucose. The sensitive response of PorPC/GOD/GCE to O_2 against H_2O_2 could be further developed for the detection of the oxidase-related substrate.

The incubation time is an important parameter for detecting glucose, the sensor was incubated in 1.0 mM glucose for different durations. From Fig. 6A, the CV peak current response of the sensor rapidly decreased with increase of incubation time from 0 to 20 min. As the quantity of O_2 was likely to have reached equilibrium in the vicinity of the modified GCE after 20 min, this was chosen as the optimal incubation time.

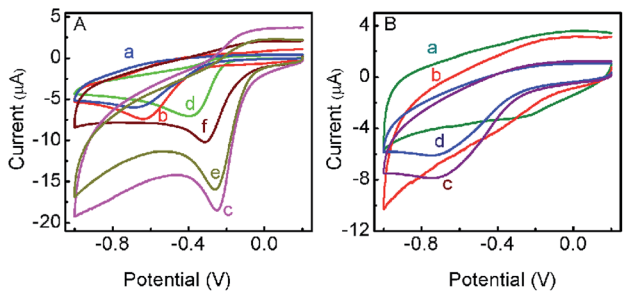

Fig. 5 (A) CVs of (a) bare GCE, (b) PC/GCE, (c) PorPC/GCE, (d) FeTCPP/GCE, (e) PorPC/GOD/GCE, and (f) (e) + 6.0 mM glucose in 0.1 M pH 7.0 air-saturated PBS. (B) CVs of (a) PorPC/GOD/GCE, (b) (a) + 2 mM H_2O_2 in nitrogen-saturated 0.1 M pH 7.0 PBS, (c) PC/GOD/GCE, and (d) (c) + 6.0 mM glucose in air-saturated PBS. The amount of PC and PorPC is 5 μg. Scan rate: 50 mV s^{-1}.

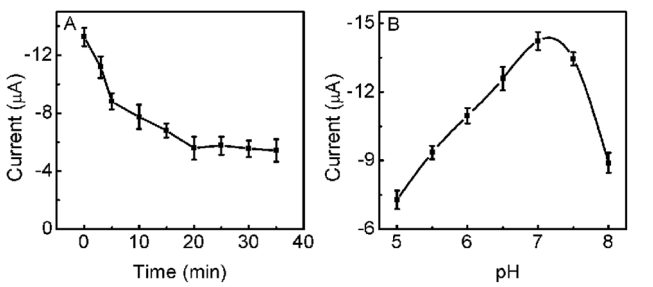

Fig. 6 (A) Effect of incubation time on the CV response to 6 mM glucose and (B) effect of pH value of the detection solution on the electrochemical signal of PorPC/GOD/GCEs in air-saturated 0.1 M pH 7.0 PBS.

Owing to the fact that both the electrochemical activity of porphyrin and biocatalytic activity of GOD are related to pH, the effect of pH on the sensor response was studied. The sensor response for 1.0 mM of glucose in buffer with different pH values was evaluated out by recording CVs. As shown in Fig. 6B, the peak current increased with the increasing pH value from 5.0 to 7.0 and decreased when the pH value increased further. Since a maximum current response occurs at pH 7.0, this value was selected as the optimum pH value for glucose measurement.

Under the optimized conditions, different concentrations of glucose solutions were analyzed and the CV current was recorded at the PorPC/GOD/GCE in air-saturated 0.1 M pH 7.0 PBS. As shown in Fig. 7, the electrocatalytic potential of the sensor increased from −0.25 V to −0.35 V with increasing glucose concentration, however, the cathodic peak current (I_{pc}) at the PorPC/GOD/GCE decreased with the increasing glucose concentration. A corresponding calibration plot with a correlation coefficient of 0.998 ($N = 10$), showing good accuracy of this method, can be represented by the expression, I_{pc} (μA) = 0.5 c (mM) − 14.8. A detection limit of 0.08 mM ($S/N = 3$) was then estimated. The linear range of the present sensor for glucose detection was better than those of the GOD/polyaniline hydrogel (0.1–2.6 mM),[66] $MnCo_2O_4$ nanofibers (0.05–800 μM),[67] and Cu_2S nanoparticles (10 μM–3.1 mM),[68] owing to the intersecting three-dimensional structure of porous carbon and the synergistic effect between good catalytic capacity of FeTCPP and excellent conductivity of porous carbon.

To exclude the potential interfering species in glucose detection, we examined the CV response to 5.0 mM AA and 5.0 mM UA at PorPC/GOD/GCEs. In comparison with 1.0 mM glucose, the CV current responses of 5.0 mM UA and 5.0 mM AA exhibited an increase of 8.4% and 4.3%, respectively, indicating the acceptable selectivity of this sensing against those interfering species due to the low operating potential. Thus this sensing strategy can be used for the detection of glucose in serum samples.

To evaluate its stability, the biosensor was employed to measure 6.0 mM glucose ten times. The relative standard deviation (RSD) was 3.9%, indicating the good stability and precision of the sensing. Further, in order to estimate the inter-assay reproducibility, ten independently prepared electrodes from the batch were used with the obtained RSD of 4.2%. When not in use, it was stored in 0.1 M PBS (pH 7.0) at 4 °C. After 6 weeks, the biosensor still retained 86% of the initial value. Therefore, the sensing strategy exhibits good operation stability, excellent fabrication reproducibility, and good durability and stability, and can be applied in real-life sample analysis.

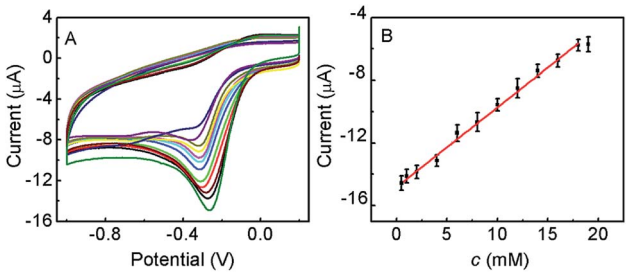

Fig. 7 (A) CVs of PorPC/GOD/GCE in 0.1 M, pH 7.0 PBS containing the glucose concentration of 0.1, 0.5, 1.0, 2.0, 4.0, 6.0, 8.0, 10, 12, 14, 16, and 18 mM from outside to inner. (B) Calibration curve of the biosensor for glucose determination at −0.25 V. Scan rate: 50 m V s^{-1}.

Table 1 Concentrations of glucose in human blood serum samples

Sample	Detection (mM)	Added (mM)	Found (mM)	Recovery (%)
1	2.72	2	5.05	106.7 ± 1.9
2	1.34	2	3.25	97.3 ± 2.4
3	1.16	2	3.37	107.7 ± 2.7
4	5.59	3	8.44	98.3 ± 2.2
5	5.49	3	8.42	99.2 ± 2.7
6	5.47	3	8.75	103.3 ± 1.7

The practical application of this sensor was carried out in serum without any need for sample pretreatment except a dilution step. The serum samples obtained from the patients were properly diluted by pH 7.0 PBS buffer when the levels of glucose were over the calibration range. A total of 6 serum samples were measured with an incubation time of 20 min and the results are shown in Table 1. The concentration of glucose was measured based on the calibration equation and the original concentration was obtained by considering the appropriate dilution ratio. When spiking with 2.0 mM and 3.0 mM glucose to real samples, the analytical recoveries are from 97.3% to 107.7%, showing good accuracy of glucose determination in real samples.

Conclusions

This work successfully designed a biomimetic catalyst by assembly of porphyrin on porous carbon derived from metal–organic frameworks for electrochemical biosensing. By employing MOFs as a template and carbon precursor, porous carbon with a high surface area and large pore volume was easily prepared by direct carbonization of ZIF-8 powders. The nitrogen heteroatoms were confirmed to be incorporated in the carbon nanomatrix. Thus this novel carbon material was conveniently functionalized with porphyrin through π–π non-covalent interactions. The hybrid nanocomposite has good dispersion in aqueous solution and excellent electrocatalytic activity toward dissolved oxygen reduction due to the synergic effect of the accelerated electron transfer and ion diffusion of porous carbon, and superior catalytic performance of porphyrin toward O_2. Coupling with the excellent bioactivity of anchored GOD, the glucose biosensor was constructed possessing good performance with a wide detection range, high detection uplimit, and acceptable stability. Moreover, the sensor was successfully used for detecting real-life serum samples without any treatment. The present findings provide us with a new example of application of the rapidly growing MOF family,

which has a potential possibility for further investigation in clinical tests.

Acknowledgements

This work was financially supported by the National Basic Research Program of China (2010CB732400), National Natural Science Foundation of China (21375060, 21121091, 21135002).

Notes and references

1 X. Q. Liu, R. Freeman, E. Golub and I. Willner, *ACS Nano*, 2011, **5**, 7648.
2 Y. J. Guo, L. Deng, J. Li, S. J. Guo, E. K. Wang and S. J. Dong, *ACS Nano*, 2011, **5**, 1282.
3 L. Z. Gao, J. Zhuang, L. Nie, J. B. Zhang, Y. Zhang, N. Gu, T. H. Wang, J. Feng, D. L. Yang, S. Perrett and X. Y. Yan, *Nat. Nanotechnol.*, 2007, **2**, 577.
4 Y. Aiba, J. Sumaoka and M. Komiyama, *Chem. Soc. Rev.*, 2011, **40**, 5657.
5 R. P. Bonarlaw and J. K. M. Sanders, *J. Am. Chem. Soc.*, 1995, **117**, 259.
6 X. Zhang, H. P. Xu, Z. Y. Dong, Y. P. Wang, J. Q. Liu and J. C. Shen, *J. Am. Chem. Soc.*, 2004, **126**, 10556.
7 Z. Y. Dong, Y. G. Wang, Y. Z. Yin and J. Q. Liu, *Curr. Opin. Colloid Interface Sci.*, 2011, **16**, 451.
8 Y. Lu, N. Yeung, N. Sieracki and N. M. Marshall, *Nature*, 2009, **460**, 855.
9 L. Pasquato, F. Rancan, P. Scrimin, F. Mancin and C. Frigeri, *Chem. Commun.*, 2000, 2253.
10 F. Manea, F. B. Houillon, L. Pasquato and P. Scrimin, *Angew. Chem., Int. Ed.*, 2004, **43**, 6165.
11 M. Comotti, C. D. Pina, R. Matarrese and M. Rossi, *Angew. Chem., Int. Ed.*, 2004, **43**, 5812.
12 F. Natalio, R. Andre, A. F. Hartog, B. Stoll, K. P. Jochum, R. Wever and W. Tremel, *Nat. Nanotechnol.*, 2012, **7**, 530.
13 Z. L. Wang, H. Y. Liu, S. H. Yang, T. Wang, C. Liu and Y. C. Cao, *Proc. Natl. Acad. Sci. U. S. A.*, 2012, **109**, 12387.
14 K. L. Fan, C. Q. Cao, Y. X. Pan, D. Lu, D. L. Yang, J. Feng, L. N. Song, M. M. Liang and X. Y. Yan, *Nat. Nanotechnol.*, 2012, **7**, 459.
15 A. Karakoti, S. Singh, J. M. Dowding, S. Seal and W. T. Self, *Chem. Soc. Rev.*, 2010, **39**, 4422.
16 J. X. Xie, X. D. Zhang, H. Wang, H. Z. Zheng and Y. M. Huang, *TrAC, Trends Anal. Chem.*, 2012, **39**, 114.
17 I. Celardo, J. Z. Pedersen, E. Traversa and L. Ghibelli, *Nanoscale*, 2011, **3**, 1411.
18 M. F. Shao, J. B. Han, W. Y. Shi, M. Wei and X. Duan, *Electrochem. Commun.*, 2010, **12**, 1077.
19 W. W. Tu, J. P. Lei, L. Ding and H. X. Ju, *Chem. Commun.*, 2009, **28**, 4227.
20 W. W. Tu, J. P. Lei and H. X. Ju, *Chem.–Eur. J.*, 2009, **15**, 779.
21 W. M. Ching, C. H. Chuang, C. W. Wu, C. H. Peng and C. H. Hung, *J. Am. Chem. Soc.*, 2009, **131**, 7952.
22 C. Berto, V. K. K. Praneeth, L. E. Goodrich and N. Lehnert, *J. Am. Chem. Soc.*, 2009, **131**, 17116.
23 Y. Liu, Y. L. Yan, J. P. Lei, F. Wu and H. X. Ju, *Electrochem. Commun.*, 2007, **9**, 2564.
24 W. W. Tu, J. P. Lei, S. Y. Zhang and H. X. Ju, *Chem.–Eur. J.*, 2010, **16**, 10771.
25 F. C. Anson, C. N. Shi and B. Steiger, *Acc. Chem. Res.*, 1997, **30**, 437.
26 Q. B. Wang, J. P. Lei, S. Y. Deng, L. Zhang and H. X. Ju, *Chem. Commun.*, 2013, **49**, 916.
27 W. W. Tu, J. P. Lei, G. Q. Jian, H. Zheng and H. X. Ju, *Chem.–Eur. J.*, 2010, **16**, 4120.
28 F. S. Vinhado, C. M. C. Prado-Manso, H. C. Sacco and Y. Iamamoto, *J. Mol. Catal. A: Chem.*, 2001, **174**, 279.
29 Z. Li, C. G. Xia and X. M. Zhang, *J. Mol. Catal. A: Chem.*, 2002, **185**, 47.
30 M. F. Shao, X. Y. Xu, J. B. Han, J. W. Zhao, W. Y. Shi, X. G. Kong, M. Wei, D. G. Evans and X. Duan, *Langmuir*, 2011, **27**, 8233.
31 M. D. Shirsat, T. Sarkar, J. Kakoullis, N. V. Myung, B. Konnanath, A. Spanias and A. Mulchandani, *J. Phys. Chem. C*, 2012, **116**, 3845.
32 K. Ariga, A. Vinu, Y. Yamauchi, Q. M. Ji and J. P. Hill, *Bull. Chem. Soc. Jpn.*, 2012, **85**, 1.
33 W. M. Xuan, C. F. Zhu, Y. Liu and Y. Cui, *Chem. Soc. Rev.*, 2012, **41**, 1677.
34 K. Ariga, S. Ishihara, H. Abe, M. Li and J. P. Hill, *J. Mater. Chem.*, 2012, **22**, 2369.
35 A. Almasoudi and R. Mokaya, *J. Mater. Chem.*, 2012, **22**, 146.
36 Y. D. Xia, G. S. Walker, D. M. Grant and R. Mokaya, *J. Am. Chem. Soc.*, 2009, **131**, 16493.
37 H. L. Jiang, B. Liu, Y. Q. Lan, K. Kuratani, T. Akita, H. Shioyama, F. Q. Zong and Q. Xu, *J. Am. Chem. Soc.*, 2011, **133**, 11854.
38 Y. Yu, L. Gu, C. B. Zhu, P. A. van Aken and J. Maier, *J. Am. Chem. Soc.*, 2009, **131**, 15984.
39 X. Y. He, L. Zhou, E. P. Nesterenko, P. N. Nesterenko, B. Paull, J. O. Omamogho, J. D. Glennon and J. H. T. Luong, *Anal. Chem.*, 2012, **84**, 2351.
40 M. Hu, J. Reboul, S. Furukawa, N. L. Torad, Q. M. Ji, P. Srinivasu, K. Ariga, S. Kitagawa and Y. Yamauchi, *J. Am. Chem. Soc.*, 2012, **134**, 2864.
41 C. Journet, W. K. Maser, P. Bernier, A. Loiseau, M. L. de la Chapelle, S. Lefrant, P. Deniard, R. Lee and J. E. Fischer, *Nature*, 1997, **388**, 756.
42 A. Thess, R. Lee, P. Nikolaev, H. Dai, P. Petit, J. Robert, C. Xu, Y. H. Lee, S. G. Kim and A. G. Rinzler, *Science*, 1996, **273**, 483.
43 B. Zheng, C. G. Lu, G. Gu, A. Makarovski, G. Finkelstein and J. Liu, *Nano Lett.*, 2002, **2**, 895.
44 A. Ahmadpour and D. D. Do, *Carbon*, 1996, **34**, 471.
45 H. B. Aiyappa, P. Pachfule, R. Banerjee and S. Kurungot, *Cryst. Growth Des.*, 2013, **13**, 4195.
46 J. Hu, H. L. Wang, Q. M. Gao and H. J. Guo, *Carbon*, 2010, **48**, 3599.
47 N. L. Torad, M. Hu, Y. Kamachi, K. Takai, M. Imura, M. Naito and Y. Yamauchi, *Chem. Commun.*, 2013, **49**, 2521.
48 J. P. Lei, R. C. Qian, P. H. Ling, L. Cui and H. X. Ju, *Trends Anal. Chem.*, 2014, **58**, 71.

49 H. X. Deng, S. Grunder, K. E. Cordova, C. Valente, H. Furukawa, M. Hmadeh, F. Gándara, A. C. Whalley, Z. Liu, S. Asahina, H. Kazumori, M. O'Keeffe, O. Terasaki, J. F. Stoddart and O. M. Yaghi, *Science*, 2012, **336**, 1018.
50 B. Liu, H. Shioyama, T. Akita and Q. Xu, *J. Am. Chem. Soc.*, 2008, **130**, 5390.
51 L. Radhakrishnan, J. Reboul, S. Furukawa, P. Srinivasu, S. Kitagawa and Y. Yamauchi, *Chem. Mater.*, 2011, **23**, 1225.
52 X. Jin, V. V. Balasubramanian, S. T. Selvan, D. P. Sawant, M. A. Chari, G. Q. Lu and A. Vinu, *Angew. Chem., Int. Ed.*, 2009, **48**, 7884.
53 K. P. Gong, F. Du, Z. H. Xia, M. Durstock and L. M. Dai, *Science*, 2009, **323**, 760.
54 A. Aijaz, N. Fujiwara and Q. Xu, *J. Am. Chem. Soc.*, 2014, **136**, 6790.
55 Y. Tang, B. L. Allen, D. R. Kauffman and A. Star, *J. Am. Chem. Soc.*, 2009, **131**, 13200.
56 J. M. Goran, J. L. Lyon and K. J. Stevenson, *Anal. Chem.*, 2011, **83**, 8123.
57 Z. H. Zhang, R. Zhang, C. C. Li, L. Yuan, P. P. Li, L. Yao and S. Q. Liu, *Electroanalysis*, 2012, **24**, 1424.
58 R. Banerjee, A. Phan, B. Wang, C. Knobler, H. Furukawa, M. O'Keeffe and O. M. Yaghi, *Science*, 2008, **319**, 939.
59 K. S. Park, Z. Ni, A. P. Cote, J. Y. Choi, R. Huang, F. J. Uribe-Romo, H. K. Chae, M. O'Keeffe and O. M. Yaghi, *Proc. Natl. Acad. Sci. U. S. A.*, 2006, **103**, 10186.
60 A. J. Amali, J. K. Sun and Q. Xu, *Chem. Commun.*, 2014, **50**, 1519.
61 H. L. Wang, Q. M. Gao and J. Hu, *J. Am. Chem. Soc.*, 2009, **131**, 7016.
62 L. F. Lai, J. R. Potts, D. Zhan, L. Wang, C. K. Poh, C. Tang, H. Gong, Z. X. Shen, J. Y. Lin and R. S. Ruoff, *Energy Environ. Sci.*, 2012, **5**, 7936.
63 T. Shari, G. Z. Hu, X. E. Jia and T. Wågberg, *ACS Nano*, 2012, **6**, 8904.
64 J. Schuster, G. He, B. Mandlmeier, T. Yim, K. T. Lee, T. Bein and L. F. Nazar, *Angew. Chem., Int. Ed.*, 2012, **51**, 3591.
65 A. J. Bard and L. R. Faulkner, *Electrochemical Methods: Fundamentals and Applications*, John Wiley & Sons, Inc., New York, 2nd edn, 2001.
66 L. J. Pan, G. H. Yu, D. Y. Zhai, H. R. Lee, W. T. Zhao, N. Liu, H. L. Wang, B. C. K. Tee, Y. Shi, Y. Cui and Z. N. Bao, *Proc. Natl. Acad. Sci. U. S. A.*, 2012, **109**, 9287.
67 Y. T. Zhang, L. Q. Luo, Z. Zhang, Y. P. Ding, S. Liu, D. M. Deng, H. B. Zhao and Y. G. Chen, *J. Mater. Chem. B*, 2014, **2**, 529.
68 S. K. Maji, A. K. Dutta, G. R. Bhadu, P. Paul, A. Mondal and B. Adhikary, *J. Mater. Chem. B*, 2013, **1**, 4127.